American Mineralogist, Volume 78, pages 391–404, 1993

The composition of lizardite *1T* and the formation of magnetite in serpentinites

David S. O'Hanley*
Department of Mineralogy, Royal Ontario Museum, Toronto, Ontario M5S 2C6, Canada
M. Darby Dyar
Department of Geological Sciences, University of Oregon, Eugene, Oregon 97403, U.S.A

Abstract

Mössbauer data were obtained from 23 samples [20 lizardite (*1T*) samples, two chrysotile samples, and one antigorite sample] taken from five geologically well-characterized serpentinites. These serpentinites represent both hydration and serpentine recrystallization in lizardite-chrysotile serpentinites. Mössbauer parameters obtained from the samples used in this study were integrated with electron microprobe and H_2O extraction yields to generate a comprehensive set of compositional data for lizardite, which was compared with modal magnetite values in the same samples.

Lizardite contains up to 70% of its Fe as Fe^{3+} in both tetrahedral and octahedral coordination. The $^{[6]}Fe^{3+}$ content shows a positive correlation with $^{[4]}Fe^{3+}$ and a negative correlation with $^{[6]}Fe^{2+}$. Substitutions of trivalent cations in both sheets are correlated and do not require cation vacancies (including H^+) to maintain charge balance. The $^{[4]}Fe/^{[6]}Fe$ and Si/Mg ratios of lizardite, chrysotile, and antigorite are different, with the $^{[4]}Fe/^{[6]}Fe$ ratio decreasing, and the Si/Mg ratio increasing from lizardite to chrysotile to antigorite.

The Fe_{tot} content and the $^{[6]}Fe/(^{[6]}Fe + Mg)$ and Fe^{3+}_{tot}/Fe_{tot} ratios of lizardite in the Jeffrey and Woodsreef serpentinites are inversely correlated with modal magnetite, indicating that f_{O_2} was internally controlled in these serpentinites. In contrast, the Fe_{tot} and the $^{[6]}Fe/(^{[6]}Fe + Mg)$ and Fe^{3+}_{tot}/Fe_{tot} ratios of lizardite in the Cassiar serpentinite exhibit either direct or inverse correlations with modal magnetite, indicating internal or external control of f_{O_2}, with f_{O_2} externally controlled early in recrystallization and internally controlled later in recrystallization. The availability of Si affects internal vs. external control of f_{O_2} because Si exchanges with $^{[4]}Fe^{3+}$ either to form or to consume magnetite during serpentine recrystallization.

Introduction

The serpentine minerals are Mg-rich trioctahedral 1:1 layer silicates, in which SiO_2, MgO, and H_2O (MSH) usually account for approximately 90–95% of each analysis. The misfit between the octahedral and tetrahedral sheets for serpentine compositions is relieved by different mechanisms in the different crystal structures (see Wicks and O'Hanley, 1988). Lizardite consists of planar layers, whereas chrysotile consists of cylindrical layers. Lizardite may be stable at lower temperatures than chrysotile in the MSH system because chrysotile has a larger entropy, attributable to the nonperiodic distribution of H bonds produced by its cylindrical structure (Wicks and Whittaker, 1975; Chernosky et al., 1988). Although samples of both lizardite and chrysotile contain Al and Fe^{3+}, lizardite exhibits a greater extent of substitution of these cations than does chrysotile (Wicks and Plant, 1979). Substitution of trivalent cations, such as Al and Fe^{3+}, for Mg and Si, produces stronger interactions between adjacent layers and increases the stability of the planar structure (Mellini, 1982). Antigorite has a modulated structure (Guggenheim and Eggleton, 1985), which reduces the number of octahedral coordination sites per number of tetrahedral coordination sites to reduce the misfit. As a result, antigorite contains slightly less H_2O (3.85 OH groups rather than 4 OH groups per 14 O atoms) and fewer octahedral cations (2.85 rather than 3 per 14 O atoms) than lizardite or chrysotile.

The relationship among serpentine minerals, magnetite, and f_{O_2} has long been the subject of controversy in the serpentine literature. Recently, Wicks and O'Hanley (1988) observed that magnetite can be a reactant, a product, or a passive agent during changes in serpentine mineral relations or texture. In the Cassiar serpentinite in north-central British Columbia, for example, the reactions lizardite = antigorite + magnetite and lizardite + magnetite = antigorite were inferred from petrographic observations, indicating that variations in μ_{O_2} may not induce changes in serpentine mineralogy. This conclusion was also reached by Frost (1985), who thought that O_2

* Present address: Department of Geological Sciences, University of Saskatchewan, Saskatoon, Saskatchewan S7N 0W0, Canada.

0003–004X/93/0304–0391$02.00

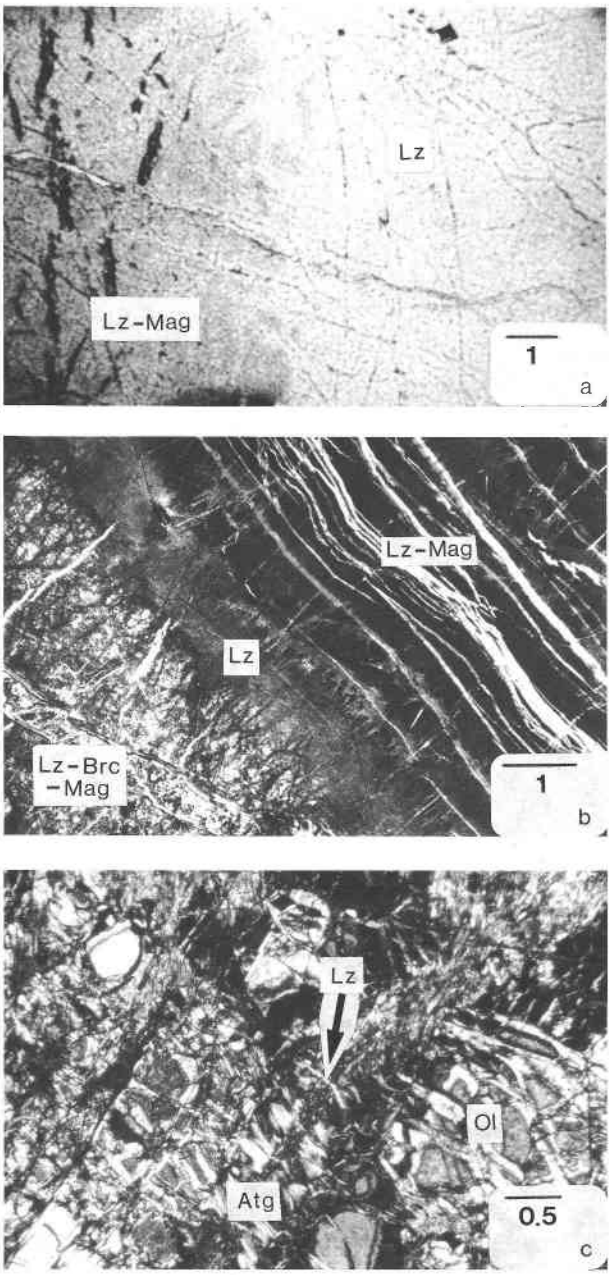

Fig. 1. Photomicrographs, all scale bars in mm. (**a**) Lizardite + magnetite (Lz-Mag) in hourglass texture, replaced by Lz ± Mag (Lz) in hourglass texture (sample J2, Jeffrey mine, Quebec). (**b**) Lz + brucite + Mag (Lz-Brc-Mag) mesh-rim texture replaced by a Lz ± Mag (Lz), low-birefringent hourglass texture, in turn replaced by a Lz + Mag (Lz-Mag) hourglass texture (W3, Woodsreef mine, New South Wales). (**c**) Olivine (Ol) cut by antigorite (Atg) mesh rims and both partly replaced by lizardite (Lz) mesh texture (arrow points to Lz replacing Atg). There is no magnetite visible in plane light (Jo21, Josephine ophiolite, California).

was too minor a component in the fluid to determine mineral assemblages. In the Jeffrey mine in southeastern Quebec, magnetite was consumed when lizardite recrystallized to form a new lizardite-bearing texture (Fig. 1a). These observations suggest that μ_{O_2} may be constant during the formation of magnetite during serpentinization. The formation of magnetite may indicate a change in the partitioning of Fe^{3+} rather than a change in μ_{O_2}, or a change in some other parameter. However, in the absence of data on the Fe^{3+} content of the serpentine minerals, the implications of these observations could not be understood.

Fe^{3+} data for serpentine minerals are available from studies that used wet-chemical methods (see Whittaker and Wicks, 1970) or, more recently, utilized Mössbauer spectroscopy (e.g., Rozenson et al., 1979). The earliest Mössbauer studies of serpentine minerals by Malysheva et al. (1976) suggested that the Fe^{3+} content in serpentine might control which of the minerals forms in a given sample, but identification of the minerals is ambiguous; the fact that three of their eight samples are labeled as loop serpentines (polygonal serpentine?) makes it difficult to interpret their results. Rozenson et al. (1979) were able to resolve peaks corresponding to Fe^{3+} in tetrahedral coordination ($^{[4]}Fe^{3+}$) for only two of their samples (an antigorite and a chrysotile sample); no $^{[4]}Fe^{3+}$ was found in lizardite.

The latter studies focused on establishing Mössbauer parameters for serpentine and on the role of Fe^{3+} content of the serpentine minerals, without considering serpentine paragenesis. Mössbauer data have not been considered when interpreting lizardite composition, assemblage, or texture, until now.

We propose a model to explain the changes in lizardite composition, based on the distribution of trivalent cations in lizardite *1T*. Our results are based on thorough characterizations of minerals from several geologically well characterized lizardite-chrysotile serpentinites associated with chrysotile asbestos deposits, using a combination of analytical techniques, including X-ray diffraction, electron microprobe analysis, Mössbauer spectroscopy, and stable isotope extraction analyses. Discussion will focus on the location and concentration of trivalent cations and Fe^{2+} and H^+ in lizardite *1T* and the relationship among lizardite composition, paragenesis, and f_{O_2}.

Geologic setting

Samples for this study were taken from well-characterized lizardite-chrysotile serpentinites from chrysotile asbestos deposits for which mineral parageneses were known from X-ray diffraction studies and for which petrologic, stable isotope, and major-element compositional data were available. The geologic and petrologic characteristics of the Cassiar, Woodsreef, and United serpentinites have been described by O'Hanley (1991). The Cassiar serpentinite, located in north-central British Columbia, is a completely serpentinized harzburgite tectonite (80–90% olivine, 20–10% enstatite, minor chromite) and is an example of serpentine recrystallization in which lizardite

TABLE 1. Mineral assemblages, modal magnetite, and mineral compositions for serpentine samples used in this study

Sample	Assemblage*	Magnetite (vol%)	Mineral*	Mineral composition**								Excess charge†
				Si	$^{[4]}Fe^{3+}$	$^{[4]}Al$	$^{[6]}Al$	Cr	$^{[6]}Fe^{3+}$	Fe^{2+}	Mg	
C50	L + A, F, CrM	0.20	L	3.84	0.06	0.10	0.15	0.02	0.05	0.06	5.73	+0.06
			A	3.84	0.07	—	0.09	0.00	0.05	0.07	5.68	
C51	L + A	0.21	L	3.82	0.09	0.09	0.13	0.03	0.09	0.05	5.75	+0.07
			A	3.86	0.08	—	0.10	0.01	0.08	0.04	5.58	
C52	L + A	0.18	L	3.83	0.07	0.10	0.14	0.02	0.07	0.04	5.76	+0.06
			A	3.84	0.09	—	0.12	0.00	0.09	0.05	5.59	
C53	L	0.03	L	3.77	0.14	0.09	0.09	0.06	0.08	0.04	5.80	0.00
C54	L	0.05	L	3.89	0.06	0.05	0.08	0.02	0.06	0.02	5.84	+0.05
C55	L	0.22	L	3.84	0.08	0.08	0.06	0.06	0.07	0.08	5.82	+0.03
C56	L, CrM	0.54	L	3.86	0.11	0.03	0.08	0.01	0.10	0.05	5.82	+0.05
C139	A, Pn, M	0.00	A	3.97	0.04	0.00	0.09	0.03	0.08	0.39	5.36	+0.16
C167	C	—	C	3.97	0.04	0.00	0.05	0.00	0.05	0.04	5.78	+0.06
C200	C	—	C	3.95	0.03	0.02	0.03	0.00	0.05	0.03	5.82	+0.03
J2a	L, M	4.76	L	3.90	0.07	0.02	0.00	0.0	0.03	0.14	5.82	−0.06
J2b	L, T, M	1.00	L	3.91	0.05	0.02	0.00	0.0	0.07	0.15	5.87	0.00
J7	L + B, T, M	0.04	L	3.98	0.05	0.00	0.03	0.0	0.01	0.13	5.81	−0.01
			B + L	0.01	0.0	—	0.0	0.0	0.00	0.09	0.89	
J32a‡	L + B, M	0.29	L + B	3.95	0.02	0.02	0.00	0.0	0.03	0.08	5.87	−0.01
J32b‡	L + B + C(vn), M	0.23	L + B	3.88	0.07	0.02	0.00	0.01	0.02	0.10	5.85	−0.06
			B + L	0.14	0.0	—	0.0	0.0	0.00	0.06	0.70	
J51	L, Ch, M	0.17	L	3.94	0.04	0.02	0.00	0.01	0.05	0.08	5.85	0.00
W22a‡	O + L + B, Ch, CrM	0.10	L + B	3.99	0.02	0.00	0.00	0.00	0.02	0.06	5.87	0.00
W26a	L	0.00	L	3.97	0.06	0.00	0.03	0.00	0.05	0.10	5.78	+0.02
W26b	L, Ch, M	0.01	L	3.97	0.09	0.00	0.10	0.07	0.09	0.07	5.59	+0.17
W41	O + L + B, T, CrM	0.49	L + B	4.01	0.02	0.00	0.04	0.0	0.03	0.08	5.94	+0.05
			B	0.0	0.0	0.00	0.0	0.0	0.0	0.13	0.85	
W68	L, Pn	0.11	L	3.94	0.03	0.03	0.00	0.00	0.07	0.14	5.81	+0.01
88DSO-1‡	L + B + C(vn), T, M	0.08	L + B	3.94	0.06	0.00	0.04	0.02	0.07	0.02	5.78	+0.07
			B + L	0.06	0.0	—	0.0	0.0	0.0	0.02	0.87	
M19804	L	0.00	L	3.94	0.06	0.00	0.01	0.0	0.01	0.0	5.94	−0.04

* L = lizardite, A = antigorite, C = chrysotile, B = brucite, T = FeNi alloy, F = ferrichromite, CrM = chromian magnetite (≈1 wt% Cr_2O_3), M = magnetite, Pn = pentlandite, Ch = magnesian ferroan chromite, vn = vein.

** Serpentines based on 14 O atoms; brucite based on 1 O atom.

† Excess charge = $^{[6]}R^{3+} - {}^{[4]}R^{3+}$.

‡ Reported analyses were corrected for brucite as an impurity.

recrystallized before it was partly replaced by chrysotile and antigorite. Brucite and FeNi alloy are absent from the serpentinite, but pentlandite and heazlewoodite are present. Primary chromite has reacted extensively both before and during serpentine recrystallization such that the serpentine minerals after olivine contain up to 0.25 Al atoms per 14 O atoms (Table 1). The samples chosen for Mössbauer analysis represent the recrystallization of lizardite to antigorite (C50–C56), chrysotile asbestos veins that cut these textures (C167 and C200), and an antigorite from the hanging-wall alteration zone, in which lizardite and magnetite were replaced by antigorite (C139).

The United mine serpentinite, located in east-central Ontario, is a completely serpentinized dunite cumulate (100% olivine) from a differentiated mafic-ultramafic sill (O'Hanley, 1988). One sample from the completely serpentinized dunite (Table 1: DSO-1) was studied. It consists of lizardite + brucite + FeNi alloy + magnetite, cut by chrysotile asbestos veins. Based on the presence of lizardite + brucite in mesh textures, serpentine recrystallization is considered to be minimal.

The Woodsreef serpentinite, located in eastern New South Wales, is a partly to completely serpentinized harzburgite tectonite (65–70% olivine, 30–25% enstatite, 5% chromite; Glen and Butt, 1981; O'Hanley and Offler, 1992). Samples were chosen from partly serpentinized peridotite (W22a, W41) and completely serpentinized peridotite with either lizardite mesh textures or lizardite hourglass and interlocking textures indicative of serpentine recrystallization (W26a, W26b, W68). Chromite is optically and texturally unaltered, and the lizardite after olivine contains very little Al or Cr (Table 1). An FeNi alloy and magnetite are present in the partly serpentinized peridotite, and brucite is found only in partly and completely serpentinized peridotites that have not undergone recrystallization. Pentlandite was observed in one sample (W68).

The Madoc serpentinite, located in the Grenville Domain of Ontario, formed by serpentinization of marble. It consists of lizardite only and lacks opaque minerals (Table 1: Royal Ontario Museum no. 19804).

The Jeffrey serpentinite, located in southeastern Quebec, is a partly to completely serpentinized and recrystallized harzburgite tectonite (85–95% olivine, 10–5% enstatite, 5% chromite) that is part of an Ordovician ophiolite (Lamarche, 1973). At the Jeffrey deposit, the patterns of serpentinization in outcrop are virtually identical to those at Woodsreef. The Jeffrey deposit is divided into five ore zones labeled 1 to 5 from east to west (Fig. 2), separated by schistose serpentine devoid of chrysotile

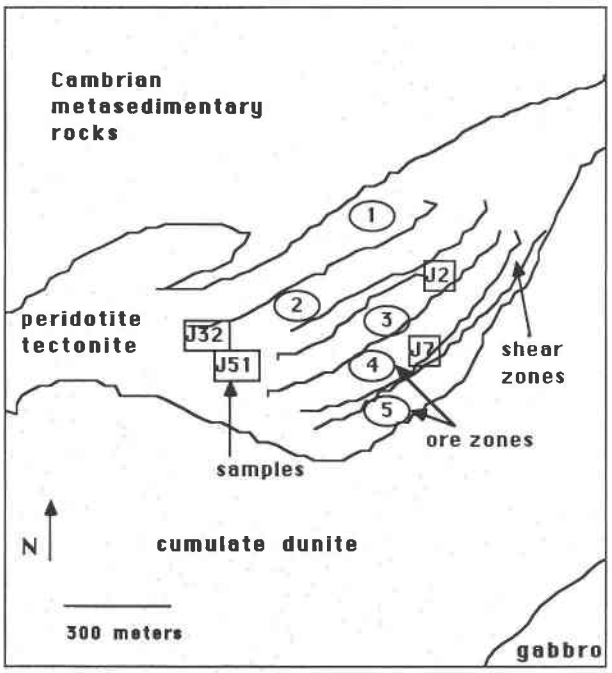

Fig. 2. Geologic sketch map of the Jeffrey mine, southeastern Quebec. Asbestos fiber is present in massive serpentinite situated in ore zones between the shear zones. The serpentinized peridotite tectonite is part of an Ordovician ophiolite.

asbestos. Although several shear zones are present within the serpentinite, the greatest extent of hydration and recrystallization occurs in the center of the serpentinite, near the boundary of ore zones 2 and 3. Sample J2 was taken from a nonschistose block of serpentinized peridotite within the shear zone between ore zones 2 and 3. Sample J7 is from ore zone 4, and samples J32 and J51 are from ore zone 2. One important feature of serpentine recrystallization in the Jeffrey serpentinite is the replacement of lizardite + chrysotile + antigorite interlocking textures by lizardite hourglass textures, particularly in ore zone 2. Chromite has reacted with serpentine in some parts of the serpentinite such that the Al and Cr contents of lizardite vary (Table 1). An FeNi alloy is present in both partly serpentinized peridotite and completely serpentinized peridotite that has not undergone recrystallization.

Experimental methods and results

Twenty-three samples were chosen from the five serpentinites. Mineral assemblages were identified optically based on the results of Wicks and Plant (1979) and by microbeam X-ray diffraction using the methodology of Wicks and Zussman (1975). The composition of opaque minerals was determined by electron microprobe. Microprobe data for the serpentine minerals were obtained using a Jeol 8600 Superprobe housed at the University of Saskatchewan; natural mineral standards, including serpentine for Mg and Si, were used under operating conditions of 15 KeV and 10 nA. Mineral assemblages, modal magnetite, and relevant compositional data (recalculated to include the Fe^{3+} data) for the lizardite samples are listed in Table 1. H_2O contents of the Cassiar lizardite samples were determined in this study using the methods and facilities described in Dyar et al. (1991), and were used in conjunction with the microprobe data (Table 1) to recalculate lizardite mineral formulas based on 18 O atoms (Table 2). Modal magnetite was determined using a Tracor-Northern Series II X-Ray Analyzer in conjunction with the microprobe. Three representative areas in each thin section were analyzed and the results averaged to obtain the value for modal magnetite given in Table 1.

The microprobe data for samples J32a, J32b, W22a, and DSO-1 have high Mg and low Si contents and Mg, Si, and Fe contents that vary with cation totals: these variations are consistent with the presence of brucite as an impurity in the lizardite in these samples. The data were corrected for brucite content by constructing regression lines for Mg, Si, and Fe vs. the total Mg + Si + Fe, using four points per grain. A specific value for the total Mg + Si + Fe was chosen by assuming a cation total of 10 (per 14 O atoms) minus the sum of all other cations present in the sample (i.e., Al, Cr, Ni, Mn). Using the determined value for Mg + Si + Fe, values for Mg, Si, and Fe were calculated from the regression curves. The corrected values for the above samples are reported in Table 1.

Mineral separates were removed from samples using thin sections to select the areas to be drilled. Purity of samples is estimated to be close to 100% serpentine + magnetite, with minor brucite or olivine impurities, as indicated in Table 1. Approximately 200–400 mg of each sample was finely ground with sugar under acetone to achieve a homogeneous thin mixture of sample across the sample holder and to minimize possible oxidation of Fe.

Mössbauer spectra were recorded in 512 channels of the constant acceleration Austin Science Associates spectrometer located in the Mineral Spectroscopy laboratory at the University of Oregon. A source of 70–20 mCi ^{57}Co in Pd and a gradient of approximately 0.01545 mm/s/channel were used. Results were calibrated against an α-Fe foil 6 mm thick and of 99.99% purity. Spectra were fitted using an IBM PC–compatible version of the program Stone (Stone et al., 1984). The program uses a Gaussian nonlinear regression procedure with the capability of constraining any set of parameters or linear combination of parameters. Lorentzian line shapes were used for resolving peaks because there was no significant improvement in fit statistics when a Gaussian component was added. Procedures used to fit individual samples were similar to those described in detail for micas by Dyar and Burns (1986).

In some cases it was necessary to fit magnetite peaks to the spectra because of the presence of magnetite as an impurity. As the velocities (i.e., peak positions) of the magnetite peaks are well known (e.g., Banerjee et al., 1967;

TABLE 2. Electron microprobe analyses and H_2O extraction yields for lizardite from the Cassiar serpentinite

Oxide	C50	C51	C52	C53	C54	C55	C56
SiO_2	40.76	39.29	40.22	38.50	40.57	39.57	40.12
Al_2O_3	2.22	1.87	2.14	1.56	1.15	1.26	0.94
Cr_2O_3	0.29	0.36	0.30	0.80	0.22	0.77	0.11
MgO	40.88	39.6	40.54	39.72	40.85	40.26	40.58
FeO*	2.18	2.81	2.13	3.18	1.73	2.07	3.22
MnO	0.05	0.05	0.04	0.07	0.06	0.10	0.04
NiO	0.18	0.18	0.18	0.17	0.16	0.17	0.16
H_2O	11.69	11.36	11.79	11.86	11.94	11.26	11.37
TOTAL**	98.27	95.55	97.34	95.89	96.71	95.51	96.63
			Mineral formula†, based on 18 O atoms				
Si	3.91	3.89	3.89	3.80	3.93	3.92	3.94
$^{[4]}Fe^{3+}$	0.07	0.09	0.07	0.13	0.06	0.08	0.11
Al	0.02	0.02	0.04	0.07	0.01	—	—
$\Sigma^{[4]}R$	4.00	4.00	4.00	4.00	4.00	4.00	4.05
Al	0.23	0.20	0.20	0.11	0.12	0.15	0.11
Cr	0.02	0.03	0.02	0.06	0.02	0.06	0.01
$^{[6]}Fe^{3+}$	0.05	0.09	0.07	0.08	0.06	0.07	0.10
Fe^{2+}	0.07	0.05	0.04	0.04	0.02	0.02	0.05
Mg	5.84	5.84	5.84	5.84	5.90	5.94	5.94
Mn	0.00	0.00	0.00	0.01	0.01	0.01	0.00
Ni	0.01	0.01	0.01	0.01	0.01	0.01	0.01
$\Sigma^{[6]}R$	6.22	6.22	6.18	6.15	6.14	6.26	6.22
H	7.48	7.50	7.60	7.81	7.71	7.43	7.44
Excess charge‡	−0.31	−0.32	−0.22	−0.14	−0.16	−0.37	−0.45
$^{[6]}Fe^{3+}/Fe^{2+}$	0.71	1.8	1.75	2.0	3.0	3.5	2.0

* Fe_{tot} as FeO.
** $TiO_2 + CoO + CaO + Na_2O + K_2O < 0.05$ wt%.
† Mössbauer data were used to partition Fe into tetrahedral and octahedral coordination sites.
‡ Assuming 18 O atoms present, because C was not measured.

Jensen and Shive, 1973), positions of those peaks were held constant in the initial models for each peak to aid in resolution of the serpentine peaks. As fitting progressed, constraints on the positions of the magnetite peaks were also removed to allow for the best possible fits, although the resolved peak positions varied little from the known positions. For most samples a minimum of 50–60 models were fitted to the spectral data to test for magnetite impurity. Ultimately a statistical best fit was obtained for each sample using the $\chi 2$ and Misfit parameters (Ruby, 1973). The practical application of these statistical parameters is discussed in Dyar (1984). At best, the precision of the Mössbauer spectrometer and the fitting procedure is approximately ±0.02 mm/s for isomer shift (δ) and quadrupole splitting (Δ) and ±1.5% of the Fe_{tot} per peak for the area of well-resolved, distinct peaks (Dyar, 1984). However, due to the heavily overlapped nature of the peaks in the serpentine spectra, the errors are estimated at ±0.05 mm/s for δ and 0.03 mm/s for Δ. The errors for the areas of the individual doublets are estimated to be ±4% of the Fe_{tot}.

DISCUSSION

Quality of the Mössbauer data

In about half of the samples, it proved impossible to separate lizardite (Fig. 3A) from finely intergrown magnetite (Fig. 3B). Therefore, it was necessary to fit the inner four magnetite peaks of the two magnetite sextets (corresponding to A and B site occupancies in magnetite) in our spectra using the procedure described above. Area data presented in Table 3 represent the peak areas of only the serpentine doublets and therefore do not always total to 100%.

All of the lizardite analyzed during this study contains $^{[4]}Fe^{3+}$, based on the high-energy peak (H_t) of the $^{[4]}Fe^{3+}$ doublet that is visible in the spectra at ±0.4 mm/s (Fig. 3A, 3B). The quality of the Mössbauer data can be assessed by plotting the velocities of the low-energy (L_t) and high-energy (H_t) peaks of the $^{[4]}Fe^{3+}$ doublet. These values are obtained from the relationships $L_t = \Delta - \delta/2$ and $H_t = \Delta + \delta/2$. The velocities group very tightly, with a width of 0.8 mm/s for both L_t and H_t (Fig. 4). Two samples plot outside this box (samples J2a and J32b), and inspection of Table 3 indicates that both samples contain significant amounts of magnetite impurity. The Mössbauer spectra for these two samples were remodeled using average values from within the L_t–H_t field, and these new parameters (Table 3, model A) were used to calculate mineral formulas in Table 1.

The Mössbauer parameters for lizardite measured in this study, which include $\delta = 1.14 \pm 0.02$ (average ± 2σ) and $\Delta = 2.73 \pm 0.14$ mm/s for $^{[6]}Fe^{2+}$, $\delta = 0.36 \pm 0.04$ and $\Delta = 0.79 \pm 0.18$ mm/s for $^{[6]}Fe^{3+}$, and $\delta = 0.21 \pm 0.04$ and $\Delta = 0.36 \pm 0.14$ mm/s for $^{[4]}Fe^{3+}$ (Table 3), are similar to those reported in the literature for other serpentines. The only lizardite spectra reported in the literature are one studied by Malysheva et al. (1976) and three studied by Rozenson et al. (1979). The peak positions in the former spectrum, which was fitted with the same three doublets found here, resemble our data for the least-recrystallized lizardite, but the sample contains significant-

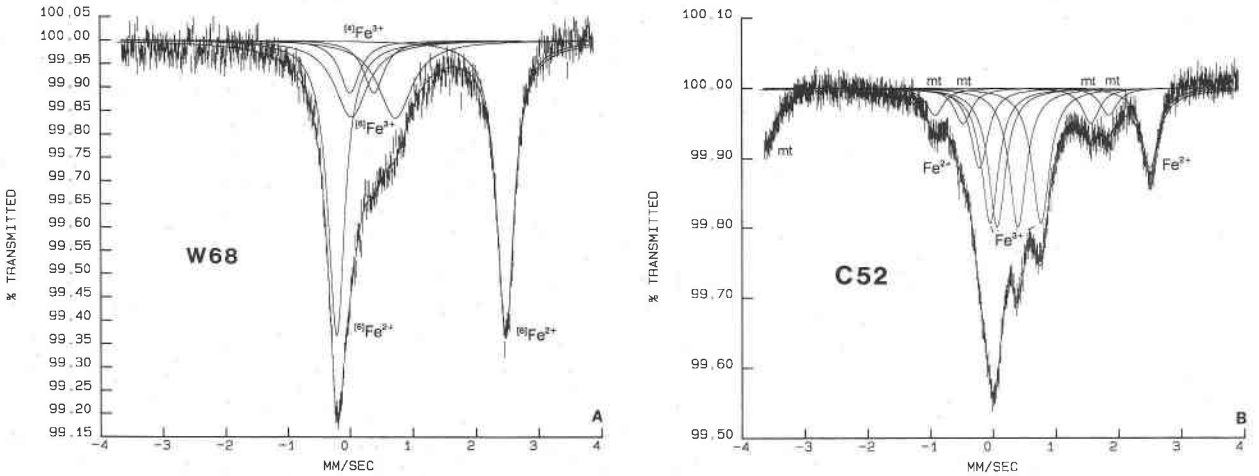

Fig. 3. Typical Mössbauer spectra of lizardite. (**A**) Sample W68 from Woodsreef yields a spectrum typical of pure lizardite; it has three doublets corresponding to $^{[6]}Fe^{2+}$, $^{[6]}Fe^{3+}$, and $^{[4]}Fe^{3+}$. (**B**) Sample C52 from Cassiar shows the more complicated spectrum of lizardite containing magnetite impurity. Five doublets are fitted to the spectrum, including two central doublets that are the innermost components of magnetite sextets. The contribution from the magnetite is most apparent at the lower end of the velocity range used in this study (visible at −3.7 mm/s in the spectrum). This region of the spectrum was not fitted because the entire magnetite peak did not lie in the region of interest to this study. The comparison of these two spectra illustrates the difficulties of studying lizardite when spectroscopically pure separates may be impossible to prepare.

ly more $^{[4]}Fe^{3+}$ (61%). Data reported by Rozenson and coworkers are difficult to interpret because peaks with $^{[4]}Fe^{3+}$ parameters were not found. For two of their three samples of lizardite, the octahedral contribution of Fe^{2+} to the spectra was split into two doublets ascribed to Fe^{2+} in M1 and M2. These fits result in two very different M1/M2 ratios (0.58 and 0.18), with a wide range of Mössbauer parameters. In our data set, two Fe^{2+} doublet fits were attempted for samples without magnetite impurities (i.e., where spectrum quality was sufficiently good to allow meaningful fits of multiple doublets). However, those fits are not reported here because (1) peak widths of the $^{[6]}Fe^{2+}$ doublets are not wide enough to suggest the presence of two rather than one doublet, and (2) when such

Table 3. Mössbauer parameters for serpentine samples

Sample	Remarks	$^{[6]}Fe^{2+}$ IS 1	QS 1	W 1	A 1	$^{[6]}Fe^{3+}$ IS 2	QS 2
Cassiar-50	interlocking texture	1.14	2.72	0.38	34	0.32	0.86
Cassiar-51	interlocking texture	1.14	2.71	0.35	19	0.36	0.82
Cassiar-52	interlocking texture	1.14	2.71	0.33	19	0.36	0.81
Cassiar-53	type 2 hourglass, ribbon and curtain	1.15	2.67	0.41	16	0.35	0.89
Cassiar-54	type ½ hourglass	1.15	2.70	0.27	14	0.38	0.76
Cassiar-55	type 2 hourglass	1.14	2.71	0.32	10	0.34	0.83
Cassiar-56	type 1 hourglass	1.12	2.70	0.38	17	0.35	0.81
Cassiar-167	bursts packages	1.13	2.71	0.25	30	0.35	0.75
Cassiar-200	doesn't burst	1.13	2.71	0.25	29	0.33	0.75
Cassiar-139	hanging wall	1.13	2.69	0.35	78	0.41	0.70
DSO-1	United mine, liz + mag mesh	1.16	2.67	0.25	10	0.38	0.63
Jeffrey-2a	liz + mag (Model A)	1.14	2.69	0.27	31	0.37	0.73
	liz + mag (Model B)	1.14	2.68	0.27	31	0.35	0.70
Jeffrey-2b	liz + mag (younger)	1.13	2.70	0.27	44	0.38	0.69
Jeffrey-7	liz + bru + mag	1.14	2.78	0.36	67	0.34	0.97
Jeffrey-32a	liz + mag	1.14	2.76	0.31	61	0.39	0.70
Jeffrey-32b	liz + bru + mag (younger) (Model A)	1.13	2.73	0.25	17	0.37	0.84
	liz + bru + mag (younger) (Model B)	1.12	2.82	0.30	17	0.40	0.61
Jeffrey-51	liz + mag	1.13	2.69	0.27	44	0.40	0.69
Woodsreef-22a	liz + mag + ol?	1.13	2.88	0.38	59	0.35	0.89
Woodsreef-41	liz + mag + ol?	1.14	2.93	0.31	60	0.36	0.83
Woodsreef-26a	hourglass	1.12	2.70	0.32	42	0.32	0.88
Woodsreef-26b	interlocking	1.13	2.71	0.39	28	0.36	0.73
Woodsreef-68	liz + mag	1.13	2.69	0.33	58	0.38	0.70
M19804	Madoc township, after limestone	—	—	—	—	0.40	0.68

* Because of the presence of >40% magnetite, fit parameters do not reflect goodness of fit and are therefore not tabulated. Error bars on these fits are at least twice those given for better purified samples.

fits were attempted, improvement in the statistical parameters of the fits was not significant. Therefore, we could not justify use of two Fe^{2+} doublets in our fits. More importantly, the refinements of lizardite *1T* by Mellini (1982) and of lizardite *1T* and lizardite $2H_1$ by Mellini and Zanazzi (1987) did not indicate the presence of two distinct octahedral sites. Accordingly, fits incorporating two doublets corresponding to different $^{[6]}Fe^{2+}$ sites are not reported here.

Most of the data reported in the literature were obtained from chrysotile and antigorite. The reported data suffer from a lack of compositional or provenance information and are of uneven quality, making them difficult to interpret. For example, chrysotile samples from the same ore grade (BC-110-4D) investigated by Blaauw et al. (1979) and Nagy-Czabo et al. (1981) resulted in two different reported results; the former group found $^{[4]}Fe^{3+}$, but the latter group did not. The fact that Nagy-Czabo et al. (1981) reported no $^{[4]}Fe^{3+}$ may be related to the probable presence of magnetite with the chrysotile, which could mask the $^{[4]}Fe^{3+}$ peak. Regardless of how this occurred, the discrepancy between the results of Blaauw et al. (1979) and Nagy-Czabo et al. (1981) calls the latter's results into question. Our results for Cassiar fiber (C167 and C200) agree with the results of Blaauw et al. (1979).

Lizardite compositions and site occupancies

The samples of lizardite *1T* studied here exhibit minor but significant concentrations of Cr, Al, and Fe (Table 1). Other cations, such as Mn, Ni, and Co, are present in such consistently small amounts (<0.03 atoms/14 O atoms) in the samples that they are not important to un-

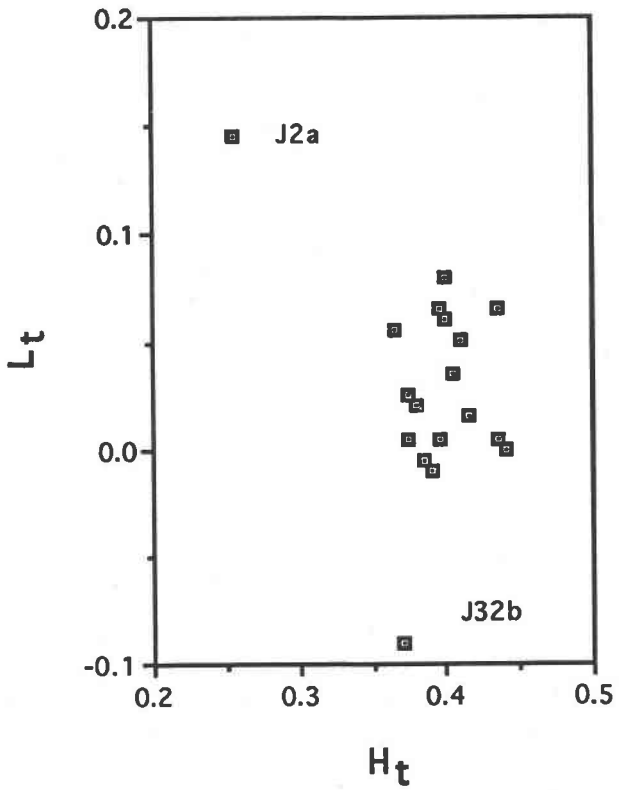

Fig. 4. A graph of the low-energy (L_t) and high-energy (H_t) peaks of the $^{[4]}Fe^{3+}$ doublet of lizardite. All points cluster in a box with widths of 0.8 mm/s, except for values for samples J2a and J32b. The Mössbauer spectra for these two samples were remodeled using values from inside the box, and the results from both models are given in Table 3.

TABLE 3. *Continued*

$^{[6]}Fe^{3+}$		$^{[4]}Fe^{3+}$									
W 2	A 2	IS 3	QS 3	W 3	A 3	%Mis	Uncert	$^{[6]}Fe^{2+}$	$^{[6]}Fe^{3+}$	$^{[4]}Fe^{3+}$	Fe^{3+}_{tot}
0.38	25	0.21	0.31	0.38	34	−2.88	−0.38	37	27	37	63
0.35	33	0.23	0.34	0.35	35	0.61	0.05	22	38	40	78
0.33	33	0.23	0.33	0.33	33	0.41	0.06	22	39	39	78
0.41	29	0.23	0.36	0.41	51	−8.40	−1.02	17	30	53	83
0.39	40	0.22	0.37	0.36	36	−0.21	−0.03	16	44	40	84
0.32	34	0.23	0.33	0.32	40	0.44	0.08	12	40	48	88
0.38	37	0.20	0.35	0.38	40	−0.12	−0.03	18	39	43	82
0.56	39	0.18	0.35	0.42	30	−0.17	−0.04	30	39	30	70
0.59	47	0.17	0.33	0.36	25	−0.34	−0.06	29	47	25	71
0.66	15	0.21	0.36	0.39	7	0.03	0.01	78	15	7	22
0.49	42	0.19	0.39	0.36	34	0.60	0.05	12	49	40	88
0.40	8	0.21	0.33	0.43	14	*	*	58	15	26	42
0.39	7	0.20	0.11	0.43	14	*	*	60	13	27	40
0.56	20	0.19	0.37	0.38	15	3.45	0.21	56	25	19	44
0.55	7	0.22	0.37	0.45	26	0.64	0.09	67	7	26	33
0.51	23	0.20	0.36	0.33	12	−0.03	−0.02	64	24	13	36
0.25	4	0.21	0.36	0.28	12	*	*	52	12	36	48
0.30	7	0.14	0.46	0.30	9	*	*	52	21	27	48
0.46	28	0.19	0.40	0.33	21	−0.24	−0.05	47	30	23	53
0.38	20	0.25	0.37	0.38	21	0.32	0.03	59	20	21	41
0.50	25	0.22	0.43	0.41	15	0.07	0.02	60	25	15	40
0.32	20	0.24	0.32	0.32	25	0.44	0.07	48	23	29	52
0.58	36	0.20	0.43	0.48	36	0.48	0.11	28	36	36	72
0.64	30	0.20	0.39	0.39	12	0.23	0.03	58	30	12	42
0.34	19	0.22	0.44	0.64	81	0.25	0.04	0	19	81	100

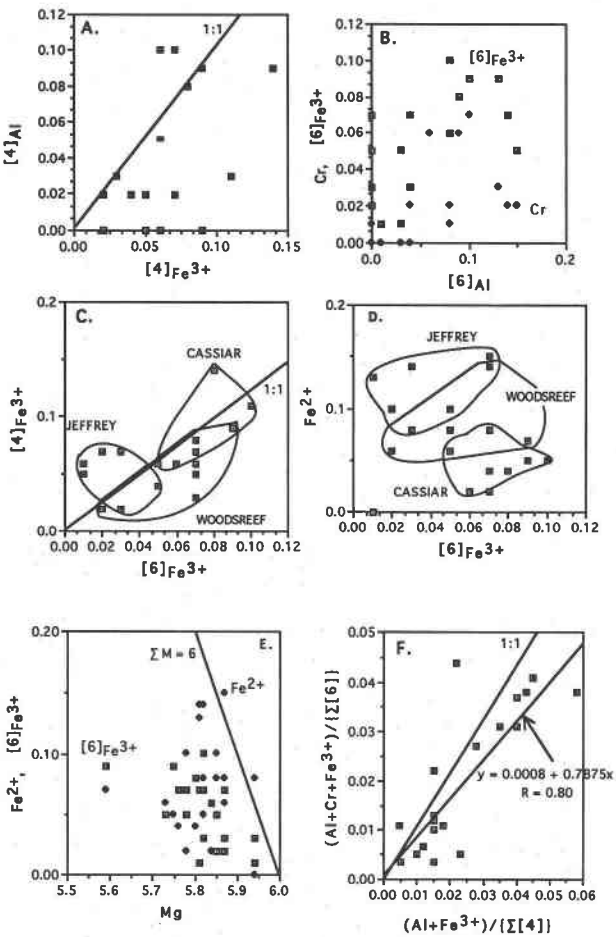

Fig. 5. Characteristics of lizardite composition as determined in this study; the data are grouped by serpentinite where appropriate. (**A**) Positive correlation of $^{[4]}$Al with $^{[4]}Fe^{3+}$: substitution of Fe^{3+} in tetrahedral sheet is slightly greater than that of Al. (**B**) Poor positive correlation of Cr and $^{[6]}Fe^{3+}$ with $^{[6]}$Al. (**C**) Positive correlation of $^{[4]}Fe^{3+}$ with $^{[6]}Fe^{3+}$. (**D**) Negative correlation of Fe^{2+} with $^{[6]}Fe^{3+}$. (**E**) Poor negative correlation of Fe^{2+} and $^{[6]}Fe^{3+}$ with Mg. (**F**) Positive correlation of ($^{[6]}$Al + Cr + $^{[6]}Fe^{3+}$)/$\Sigma^{[6]}$R (octahedral cations) with ($^{[4]}$Al + $^{[4]}Fe^{3+}$)/$\Sigma^{[4]}$R (tetrahedral cations): least-squares fit of the data goes through the origin, with a slope a little greater than the value of 0.68 expected for equal amounts of coupled substitutions of trivalent cations into both tetrahedral and octahedral sheets.

derstanding them. On the basis of the discussion above, we focus on substitutions involving Cr, Fe, and Al with Mg and Si.

The extent of cation substitution in lizardite is known to be minimal, and our data reveal no exceptions. The limited cation substitution in natural lizardite is caused by the limited range in bulk-rock compositions of serpentinites rather than limits imposed on substitution by the serpentine crystal structures, although the different serpentine minerals exhibit different extents of cation substitution (Whittaker and Wicks, 1970; Wicks and Plant, 1979). Thus, the composition of lizardite depends more on bulk-rock composition than on *P, T,* and chemical potentials. However, as our data set includes the oxidation state and site occupancies of Fe in lizardite, we can evaluate the compositional variations in natural lizardite more completely than previous workers and assess the relationship between lizardite composition and modal magnetite.

Fe^{3+} and Al occupy both tetrahedral and octahedral coordination sites in lizardite *1T* (Table 1). Fe^{3+} and Al exhibit a poor positive correlation in the tetrahedral site (Fig. 5A) and, along with Cr, a poor positive correlation in the octahedral site (Fig. 5B). Both $^{[4]}Fe^{3+}$ and $^{[6]}Fe^{3+}$ exhibit a positive correlation (Fig. 5C), whereas $^{[6]}Fe^{3+}$ and Fe^{2+} exhibit a negative correlation in the octahedral site (Fig. 5D). Both $^{[6]}Fe^{3+}$ and Fe^{2+} exhibit a poor negative correlation with Mg (Fig. 5E). Other compositional variations among the lizardite samples studied are similar to those found by Wicks and Plant (1979).

As shown in Table 1, trivalent cations occupy both tetrahedral and octahedral coordination sites in lizardite, and the charge imbalance that results from the substitution of Fe^{3+} and Al for Si, and Fe^{3+}, Al, and Cr for Mg is very small. A graph of (Al + Cr + Fe^{3+})/$\Sigma^{[6]}$R (octahedral cations) vs. (Al + Fe^{3+})/$\Sigma^{[4]}$R (tetrahedral cations) shows that the data yield a regression line with a slope <1 that passes through the origin (Fig. 5F). The trend of the data suggests that the substitution of trivalent cations in these lizardite samples occurs without the formation of cation vacancies for two reasons. First, the line passes through the origin, and second, equal amounts of substitution of trivalent cations into both the tetrahedral and octahedral sheets will result in a line with a slope equal to 0.68, which is very close to the calculated value of 0.79.

The data presented above lead to several conclusions regarding the composition of lizardite. First, Fe^{3+} occupies both tetrahedral and octahedral coordination sites in lizardite, so that both Fe^{3+} and Al are secondary tetrahedral cations in lizardite. Second, Fe^{3+} occupies an octahedral site partly at the expense of Fe^{2+}. Third, Fe^{2+}/Mg ratios do not vary much (0.01–0.02), casting doubt on the validity of prior conclusions regarding lizardite composition based on Fe/Mg values calculated from probe data only. Finally, trivalent cation substitution in lizardite occurs such that the charge balance of the layer is maintained without the formation of cation vacancies.

Variations in H^+ in lizardite

The presence of unequal amounts of Fe^{3+}, Al, and Cr in the tetrahedral and octahedral sheets of the lizardite structure raises the possibility that cation vacancies (including H^+) are necessary to maintain charge balance. For example, if the octahedral sheet contains greater substitution of trivalent cations than does the tetrahedral sheet, then cation vacancies will be necessary to establish charge balance.

This premise can be tested in two ways. One way is to

plot excess charge of the structure vs. the extent of trivalent cation substitution in either the tetrahedral or the octahedral sheet. If the extent of substitution correlates positively with excess charge, then vacancies are needed to maintain charge balance. The other way to test for vacancies is to measure the H^+ content and recalculate the chemical formula; for lizardite, this means that 18 O atoms rather than 14 O atoms would be used to calculate the chemical formula.

Using the microprobe data in Table 1 (normalized to 14 O atoms), the extent of substitution of trivalent cations in the octahedral sheet is plotted vs. the excess charge (Fig. 6A), with distinctions made among samples from the different serpentinites. The lizardite samples from the Jeffrey serpentinite possess either balanced charge or negative excess charge, indicating that the structures are either charge balanced or possess a greater extent of trivalent cation substitution in the tetrahedral sheet. Both the Woodsreef and the Cassiar lizardites are either charge balanced or possess excess positive charge, which indicates a greater extent of trivalent cation substitution in the octahedral sheet. The Cassiar lizardite samples plot directly above the Woodsreef lizardite, indicating that both lizardite samples possess the same extent of excess charge for different amounts of trivalent cation substitution.

H_2O analyses were obtained for the lizardite from the Cassiar serpentinite and used in conjunction with the probe data in Table 1 to recalculate mineral formulas based on 18 O atoms (Table 2). The totals of 11.3–11.9 wt% H_2O are less than the theoretical value of 13 wt%, and the low H_2O yields lead to an excess of octahedral cations (6.1–6.3) and an excess negative charge (−0.2–−0.5 units) for the structure. These two features, together with the observation that the probe data indicate that the structure is closely charge balanced, suggest that the H_2O determinations are low because of impurities. A graph of H^+ vs. modal magnetite (Fig. 6B) suggests that the cause of the low H_2O yields is the presence of magnetite as an impurity.

Alternative explanations for the correlation of H^+ and modal magnetite and the absence of cation vacancies in lizardite are that the correlation is real and that the microprobe data, in addition to summing to low totals (84–86 wt% oxides, without H_2O), are not accurate enough to show the effect, or that O vacancies are present and the assumption of 18 O atoms is incorrect.

Given these caveats, the microprobe data and the H_2O analyses support two conclusions regarding the need for cation vacancies in lizardite. Firstly, the extent of trivalent cation substitution in the octahedral sheet is closely balanced by the extent of trivalent cation substitution in the tetrahedral sheet, so that cation or H^+ vacancies are not needed to establish charge balance. Secondly, the excess charge is <0.1 unit of charge (with sample W26b the only exception). This value is equivalent to 0.1 H^+ ions per 14 O atoms, and given that lizardite contains 8 H^+ ions per 14 O atoms, the difference of 0.1 H^+ ion, or 1%

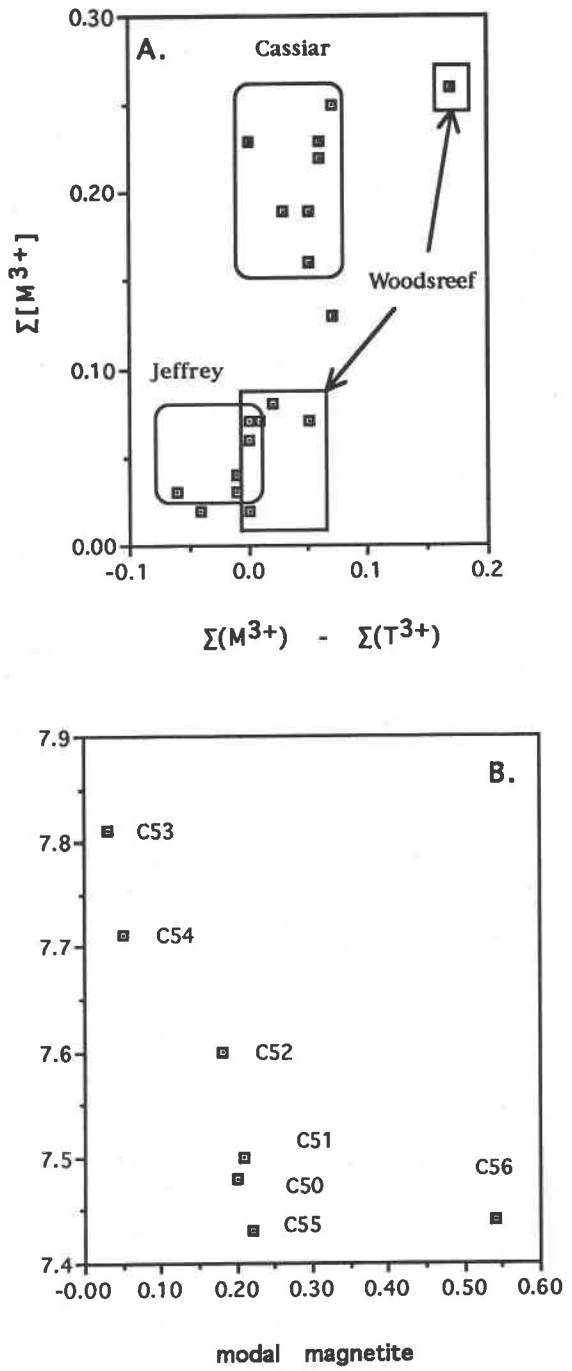

Fig. 6. (A) Graph of trivalent cation substitution in the octahedral sheet $[\Sigma^{[6]}R^{3+}]$ with excess charge on the structure $(\Sigma^{[6]}R^{3+} - \Sigma^{[4]}R^{3+})$, illustrating the lack of any correlation between the two parameters. (B) Graph of H^+/18 O atoms with modal magnetite: the negative correlation suggests that magnetite impurity in lizardite results in lower H_2O yields from the H extraction lines.

TABLE 4. Variations in modal magnetite and the amount and oxidation state of Fe in lizardite from successive assemblages

Sample	Age*	Modal magnetite	$^{[6]}Fe/(Mg + {}^{[6]}Fe)$	Fe_{tot}^{**}	Fe_{tot}^{3+}/Fe_{tot}
J2b	young	1.00	0.036	0.27	0.444
J2a	old	4.76	0.028	0.24	0.417
J32b	young	0.23	0.020	0.19	0.900
J32a	old	0.29	0.018	0.13	0.385
W26b	old	0.01	0.028	0.23	0.720
W26a	young	0.22 (vn)	0.025	0.21	0.524

* Age refers to relative age of assemblage based on one assemblage (young) replacing another (old).
** Per 14 O atoms.

of the total H^+ ions, is not resolvable with the greater uncertainty in the H_2O analyses.

Lizardite compositions and variations in modal magnetite

The variation in modal magnetite in lizardite-chrysotile serpentinites can be substantial; from no magnetite, as in sample M19804, to so much magnetite, as in some of the Woodsreef samples (Fig. 1b; samples not used in this study), that one cannot separate a sufficient amount of lizardite to analyze with the Mössbauer spectrometer.

The variations in modal magnetite and the composition of lizardite can be studied by determining how each varies in successive assemblages from the same hand sample. Three samples (J2, J32, and W26) were found in which one lizardite assemblage overprinted an earlier lizardite assemblage (Table 4; Fig. 1a). Three parameters involving the Fe content of lizardite vary consistently with modal magnetite: as modal magnetite increases, the Fe_{tot} content and the $^{[6]}Fe/(^{[6]}Fe + Mg)$ and Fe_{tot}^{3+}/Fe_{tot} ratios of lizardite decrease. These results indicate that when modal magnetite increases, the Fe content of lizardite decreases, and the Fe^{3+} content of lizardite decreases more than that of Fe^{2+}.

Note that all three samples in Table 4 formed during serpentine recrystallization, in which one lizardite assemblage replaced another, rather than during hydration, so the observed relationships between lizardite composition and modal magnetite may not apply to lizardite and magnetite formed during hydration. To determine if these results can be generalized, we first concentrate on compositional variations in lizardite vs. modal magnetite in the individual serpentinite bodies. Arrows are used to connect successive assemblages in Figures 7 and 8, with the arrow pointing from the older to the younger assemblage. The data are discussed first by deposit (Jeffrey, Woodsreef, Cassiar), and then as one data set.

The data for the lizardite samples from the Jeffrey mine are shown in Figure 7A Fe_{tot}, 7B $[^{[6]}Fe/(^{[6]}Fe + Mg)]$, and 7C Fe_{tot}^{3+}/Fe_{tot}. The arrows connect successive assemblages in two of the samples (J2, J32) given in Table 4. In all three diagrams, the arrows have negative slopes, indicating that the formation of magnetite is accompanied by a decrease in the Fe content of lizardite.

The data for the lizardite from the Woodsreef serpentinite show similar trends to those of the Jeffrey data, but the arrows point toward greater values for modal magnetite. As modal magnetite increases, Fe_{tot} (Fig. 7D), the $^{[6]}Fe/(^{[6]}Fe + Mg)$ (Fig. 7E), and Fe_{tot}^{3+}/Fe_{tot} (Fig. 7F) ratios decrease.

The lizardite from the Cassiar mine represents the recrystallization of lizardite (C53–C56) through to the formation of lizardite + antigorite (C50–C52). The arrows in Figure 8A, 8B, and 8C represent the sequence from the least- to the most-recrystallized sample. In each of the three diagrams it is apparent that there are two trends. The arrows that connect samples C54–C56 have positive slopes, indicating that both modal magnetite and the Fe content of lizardite decrease with an increase in the extent of recrystallization. The situation changes from samples C54–C52, in which the arrows have negative slopes, indicating that modal magnetite increases as the Fe content of lizardite decreases. The arrows for samples C52–C50 are almost vertical, indicating that the composition of lizardite changes without affecting modal magnetite. As antigorite is present in these three samples, we think that the changes in the Fe content of lizardite that are not related to modal magnetite are related to the formation of antigorite.

Although the data from the three serpentinites indicate that there is a relationship between the composition of lizardite and modal magnetite, a general trend is not apparent when all the data are treated as one data set (Fig. 8D–8F). This is because the relationship between the Fe content of lizardite and modal magnetite exhibits both negative and positive correlations, depending on the example, and because the variation in modal magnetite is small when compared with the variations in the Fe content of lizardite.

The control of f_{O_2} during serpentinization

According to Frost (1991), if f_{O_2} is internally controlled by silicate minerals in the silicate + oxide assemblage, then the Fe/(Fe + Mg) ratio of the silicates should be inversely correlated with modal magnetite because the Fe to form magnetite is supplied from the silicates. If modal magnetite increases, the Fe content of the silicates should decrease. If f_{O_2} is externally controlled, the opposite relationship should be observed; that is, the Fe content of the silicates should be positively correlated with modal magnetite because Fe must be added to the rock to increase the Fe content of the silicates and modal magnetite. The situation is more complex in silicates that accept Fe^{3+} because of the coupled substitutions that are needed to maintain charge balance.

The data suggest that f_{O_2} was internally controlled during recrystallization in the Woodsreef and Jeffrey serpentinites. The situation was more complex at Cassiar. At the start of recrystallization, the data suggest that f_{O_2} was externally controlled, but during recrystallization f_{O_2} was

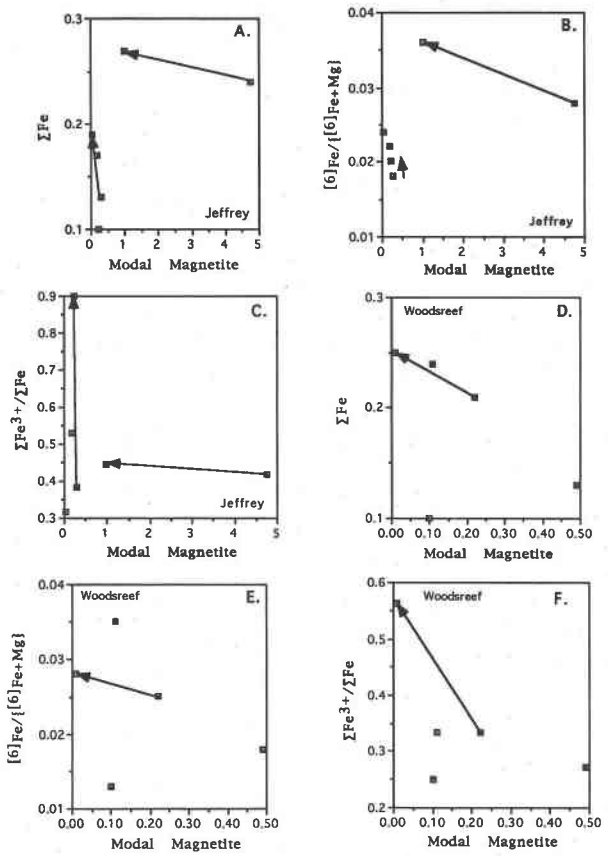

Fig. 7. Graphs of Fe_{tot}, $^{[6]}Fe/(^{[6]}Fe + Mg)$, and Fe^{3+}_{tot}/Fe_{tot} vs. modal magnetite for the Jeffrey (**A–C**) and Woodsreef (**D–F**) samples. The arrows connect successive assemblages in the same hand sample, with the arrow pointing towards the younger assemblage. The data indicate all three parameters are inversely correlated with modal magnetite.

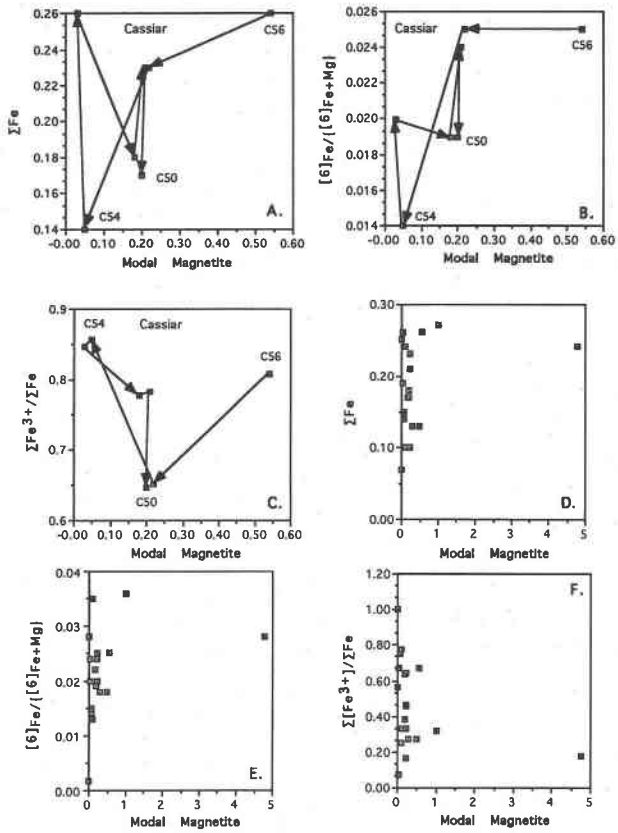

Fig. 8. Graphs of Fe_{tot}, $^{[6]}Fe/(^{[6]}Fe + Mg)$, and Fe^{3+}_{tot}/Fe_{tot} vs. modal magnetite for the Cassiar (**A–C**) samples, and for all the samples used in this study (**D–F**). For the Cassiar samples, the arrows connect successive assemblages in different hand samples, with the arrow pointing toward the younger assemblage. See text for discussion.

internally controlled. Modal magnetite was not greatly affected when lizardite was partly replaced by antigorite.

The relationships given above suggest that two different Fe end-member reactions describe the changes in lizardite composition and modal magnetite during serpentine recrystallization. These reactions are not strictly correct because greenalite $[Fe_3Si_2O_5(OH)_4]$ does not have the lizardite structure, but they do illustrate the chemical relationships, and because the extent of substitution of Fe for Mg in lizardite is small, the Fe end-member component is minor. In the first reaction, the Fe content of lizardite decreases as modal magnetite increases. This reaction most closely approximates an internal control on f_{O_2}:

$$\underset{\text{lizardite}}{Fe^{2+}_2Fe^{3+}_2SiO_5(OH)_4} + Si(OH)_4 + 0.34O_2 = \underset{\text{lizardite}}{Fe^{2+}_3Si_2O_5(OH)_4} + \underset{\text{magnetite}}{0.33Fe_3O_4} + 2H_2O.$$

The addition of Si is necessary for mass balance, but the Fe needed to form magnetite is supplied internally by lizardite.

For the examples from Cassiar in which both the Fe content of lizardite and modal magnetite increase, the Fe end-member reaction must have a source of Fe in addition to the silicates. Furthermore, lizardite with magnetite should have more Fe^{3+} than lizardite without magnetite. An Fe end-member reaction describing the addition of Fe to a lizardite + magnetite assemblage that satisfies these requirements is

$$\underset{\text{lizardite}}{Fe^{2+}_3Si_2O_5(OH)_4} + 2Fe^{2+} + 0.67O_2 = \underset{\text{lizardite}}{Fe^{2+}_2Fe^{3+}_2SiO_5(OH)_4} + \underset{\text{magnetite}}{0.33Fe_3O_4} + Si^{4+}.$$

The data and interpretations presented here indicate that f_{O_2} is neither solely internally nor solely externally controlled during serpentine recrystallization because one

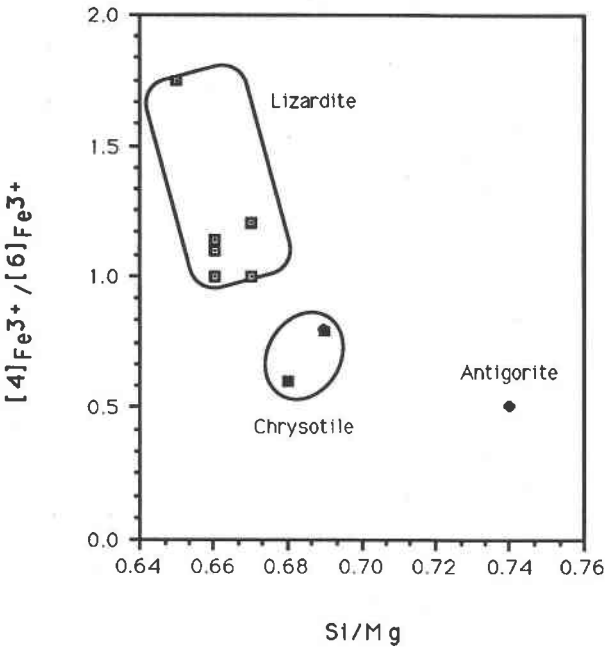

Fig. 9. Graph of $^{[4]}Fe^{3+}/^{[6]}Fe^{3+}$ vs. Si/Mg for the monomineralic serpentine samples from the Cassiar serpentinite, illustrating that the $^{[4]}Fe^{3+}/^{[6]}Fe^{3+}$ ratio decreases and the Si/Mg ratio increases from lizardite through chrysotile to antigorite.

cannot write a buffer reaction containing only O and minerals. However, in some examples of recrystallization the control on f_{O_2} is more or less internally or externally controlled, and knowledge of the serpentine paragenesis is crucial to determine which situation applies because the addition or removal of Si determines the relationship between lizardite composition and modal magnetite.

Implications for serpentinization

Stability of the serpentine minerals

It has been accepted since the work of Evans et al. (1976) that in the MSH system antigorite is stable at higher temperatures than chrysotile. Lizardite may have a stability field at lower temperatures and higher pressures than chrysotile (Chernosky et al., 1988), but this interpretation remains to be established firmly with either geologic or geochemical data. Lizardite is stabilized to higher temperatures by Al in phase equilibrium experiments, but the amount of Al used (3.5 and 9 wt% Al_2O_3; Caruso and Chernosky, 1979) is much greater than that found in most lizardite (<1 wt% Al_2O_3; Wicks and Plant, 1979). In serpentinites, lizardite is generally thought to be metastable and to form by a topotactic reaction after olivine and enstatite (Dungan, 1977). However, Wicks and Plant (1979) identified serpentinites in which the three serpentine minerals formed at the same time, indicating that lizardite recrystallized to form a new texture before it reacted to form chrysotile or antigorite (or both). Furthermore, the formation of lizardite after chrysotile, antigorite, and chlorite in the Cassiar serpentinite (O'Hanley and Wicks, 1987), and the formation of lizardite after chrysotile and antigorite in the Jeffrey mine, suggest that lizardite does have a stability field. Coupled with the inference from stable isotope studies that recrystallization occurs isothermally (O'Hanley, 1991), this sequence implies that the replacement of one serpentine mineral by another depends on composition. In the Garrison serpentinite, located in the Abitibi greenstone belt of Ontario, the replacement of lizardite by chrysotile occurs with no change in composition (O'Hanley, 1991), according to the electron microprobe data, although Fe^{3+}/Fe^{2+} ratios are not generally obtainable using that method.

Whittaker and Wicks (1970) were the first to suggest that lizardite has a preference for Fe^{3+} over chrysotile and antigorite, based on wet-chemical analyses. They used a restricted data set because they rejected many analyses that were based on the lack of identification of the serpentine, that were incomplete, and that showed the presence of impurities. If we use only the Cassiar samples that contain one serpentine mineral (Table 1), it is evident that lizardite has higher $^{[4]}Fe^{3+}/^{[6]}Fe^{3+}$ and lower Si/Mg ratios than either the antigorite or the two chrysotile samples (Fig. 9) and that chrysotile has higher $^{[4]}Fe^{3+}/^{[6]}Fe^{3+}$ and lower Si/Mg ratios than antigorite. We suggest that it is differences in these ratios among the three serpentine minerals that are related to their stability during serpentine recrystallization, as inferred from petrographic observations by O'Hanley (1991) and O'Hanley and Offler (1992), and that lizardite and chrysotile are stabilized to higher temperatures by Fe^{3+}.

The formation of magnetite in serpentinites

The serpentinization of olivine is accompanied by both the oxidation of Fe^{2+} to Fe^{3+} and the reduction of Fe^{2+} to Fe^0 (Frost, 1985). As both Fe^{2+} and Fe^{3+} can be present in lizardite, the formation of magnetite is not a necessary consequence of the serpentinization process. For example, serpentinite consisting of lizardite after antigorite and olivine, without visible magnetite, occurs in the Josephine ophiolite of northern California (Fig. 1c). The sample from the Madoc serpentinite is an extreme example of the ability of lizardite to accept Fe^{3+} such that magnetite does not form.

The substitution of Fe^{3+} for Si in the tetrahedral sheet of lizardite suggests that bulk-rock compositions with higher SiO_2 contents, like harzburgite (olivine + enstatite), should contain more magnetite than those with lower SiO_2 contents (such as dunite) because the solubility of Si in lizardite is greater than that of Fe^{3+}. The association of more modal magnetite in serpentine after harzburgite (0.42 ± 0.10 modal%) rather than serpentine after dunite (0.22 ± 0.09 modal%) was noted by Coleman and Keith (1971). In addition, brucite that forms early in the serpentinization process can be consumed later in the process, if a source of silica is present. For example, enstatite hydrates more slowly than olivine (Coleman and Keith, 1971), and then only lizardite is produced (Wicks and

Plant, 1979). The excess SiO_2 would become available later in the hydration process, after olivine had hydrated to produce lizardite + brucite. The additional Si would combine with brucite to form more lizardite and would liberate Fe to form more magnetite (O'Hanley and Offler, 1992). An Fe end-member reaction that describes this process is

$$\underset{\text{lizardite}}{Fe_3^{2+}Si_2O_5(OH)_4} + \underset{\text{brucite}}{6Fe(OH)_2} + 2SiO_2 + 0.5O_2$$
$$= \underset{\text{lizardite}}{2Fe_3^{2+}Si_2O_5(OH)_4} + \underset{\text{magnetite}}{Fe_3O_4} + 4H_2O.$$

The formation of magnetite late in the serpentinization process explains the density susceptibility data for serpentinites as well, in which density decreases more rapidly than susceptibility values increase (Toft et al., 1990). Conventional models of the serpentinization process, in which lizardite contains no Fe, or only Fe^{2+}, produce too much magnetite too early, resulting in susceptibility values that are too high for the calculated density. Solubility of Fe^{3+} in lizardite and the suppression of magnetite formation early in the serpentinization of peridotite accounts for the lag between changes in density and susceptibility.

These observations indicate that magnetic susceptibility is not a reliable criterion of the extent of serpentinization. Nor is it a reliable criterion of the extent of serpentine recrystallization because modal magnetite may actually decrease with an increase in the extent of recrystallization, as shown by samples from both Woodsreef and Cassiar.

The addition of SiO_2 during serpentine recrystallization in the ore zone in the Cassiar serpentinite probably contributed to the formation of talc, antigorite, and magnetite from lizardite, because antigorite contains more Si per 14 O atoms than does lizardite. The Fe end-member reaction given below, balanced on Fe, describes the formation of antigorite + magnetite from lizardite:

$$\underset{\text{lizardite}}{0.96Fe_3^{2+}Si_2O_5(OH)_4} + 0.05O_2 + 0.08SiO_2$$
$$= \underset{\text{antigorite}}{Fe_{2.85}^{2+}Si_2O_5(OH)_{3.7}} + \underset{\text{magnetite}}{0.01Fe_3O_4} + 0.07H_2O.$$

However, the formation at Cassiar of antigorite from lizardite + magnetite in the hanging-wall alteration zone is accompanied by a net reduction of Fe^{3+} to Fe^{2+}, on the basis of the petrographic observations of antigorite forming from lizardite, magnetite, and pentlandite, and the Mössbauer data on sample C139 (Table 1), which indicates that antigorite in this sample contains mostly Fe^{2+}.

This discussion on the stability of the serpentine minerals implies that the $^{[4]}Fe^{3+}/^{[6]}Fe^{3+}$ and Si/Mg ratios of the serpentine minerals are important in the stability of the serpentine minerals, so that the serpentine minerals are not polymorphs in general, although lizardite, chrysotile, and antigorite may have similar compositions in specific situations. The $^{[4]}Fe^{3+}/^{[6]}Fe^{3+}$ and Si/Mg ratios of the lizardite samples used in this study are shown in Figure 10, along with the values for the chrysotile and antigorite samples. Also indicated are those samples that contain Fe alloy or brucite (or both); almost all of the samples contain magnetite.

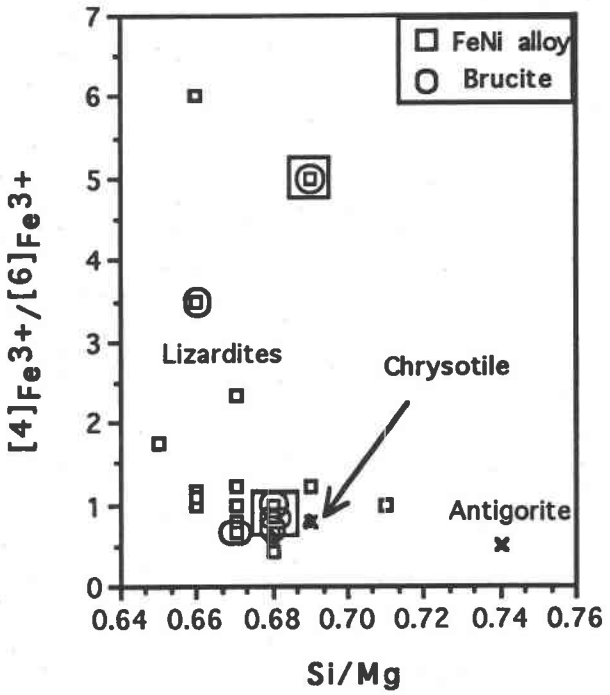

Fig. 10. Graph of $^{[4]}Fe^{3+}/^{[6]}Fe^{3+}$ vs. Si/Mg for all the samples used in this study, including the chrysotile and antigorite samples. Samples containing brucite or Fe alloy (or both) are indicated.

There are exceptions to any conclusions drawn from these data because of the scatter within them. However, samples with brucite and Fe alloy (+ magnetite) plot at Si/Mg ratios of 2.68–2.69, just above the ideal Si/Mg ratio of 2.67 for serpentine. Samples with brucite (and without Fe alloy) plot at lower Si/Mg ratios than samples with Fe alloy and brucite. There is no clear relationship between lizardite composition and modal magnetite, although samples with high $^{[4]}Fe^{3+}/^{[6]}Fe^{3+}$ and high Si/Mg ratios tend to have less modal magnetite than those samples with low $^{[4]}Fe^{3+}/^{[6]}Fe^{3+}$ and low Si/Mg ratios.

The identification of FeNi alloy in completely serpentinized peridotite (J2b, J7, 88DSO-1) is contrary to the prediction by Frost (1985) that FeNi alloy is stabilized at low f_{O_2} values by the isobaric-isothermal reaction

$$\underset{\text{olivine}}{20Fe_2SiO_4} + 22H_2 + 3O_2$$
$$= \underset{\text{serpentine}}{10Fe_3Si_2O_5(OH)_4} + \underset{\text{brucite}}{2Fe(OH)_2} + \underset{\text{magnetite}}{2Fe_3O_4} + \underset{\text{alloy}}{2Fe}$$

in which the presence of olivine with the other phases buffers f_{O_2} at values equivalent to the iron-magnetite (IM)

buffer. According to Frost (1985), once olivine reacts out during hydration, f_{O_2} should increase markedly. As serpentinites that have not undergone recrystallization contain brucite as well as FeNi alloy, we propose the following Fe end-member reaction

$$\underset{\text{brucite}}{4Fe(OH)_2} = \underset{\text{alloy}}{Fe} + 4H_2 + 2O_2 + \underset{\text{magnetite}}{Fe_3O_4}$$

as a reaction that operates in unrecrystallized serpentinites to buffer f_{O_2} at values equivalent to the IM buffer. Many serpentinites that have undergone serpentine recrystallization lack both brucite and FeNi alloy; therefore f_{O_2} should be higher in this type of serpentinite.

Acknowledgments

The authors thank Greg and Ber Harper and S.U.N.Y. Gasquet for inspiration and accommodation during this collaboration. M.D.D. acknowledges the support of NSF grants EAR-8709359 and EAR-8816935. D.S.O. thanks JM Asbestos Inc. for permission to use the Jeffrey samples and the Asbestos Institute for supporting research in the Jeffrey mine. D.S.O. also thanks Randy George of the Department of Geological Sciences of the University of Saskatchewan for assistance on the electron microprobe. Finally, we thank Fred Wicks (Royal Ontario Museum), Joe Chernosky (University of Maine), and Dave Bish (Los Alamos National Laboratory) for their comments on the manuscript.

References cited

Banerjee, S.K., O'Reilly, W.E., and Johnson, C.E. (1967) Mössbauer effect measurements in FeTi spinels with local disorder. Journal of Applied Physics, 38, 1289–1293.

Blaauw, C., Stroink, G., Leiper, W., and Zentilli, M. (1979) Mössbauer analysis of some Canadian chrysotiles. Canadian Mineralogist, 17, 713–717.

Caruso, L.J., and Chernosky, J.V., Jr. (1979) The stability of lizardite. Canadian Mineralogist, 17, 757–769.

Chernosky, J.V., Jr., Berman, R.G., and Bryndzia, L.T. (1988) Stability, phase relations, and thermodynamic properties of chlorite and serpentine group minerals. In Mineralogical Society of America Reviews in Mineralogy, 19, 295–346.

Coleman, R.G., and Keith, T.E. (1971) A chemical study of serpentinization—Burro Mountain, California. Journal of Petrology, 12, 173–183.

Dungan, M. (1977) Metastability in serpentine-olivine equilibria. American Mineralogist, 62, 1018–1029.

Dyar, M.D. (1984) Precision and interlaboratory reproducibility of measurements of the Mössbauer effect in minerals. American Mineralogist, 72, 102–112.

Dyar, M.D., and Burns, R.G. (1986) Mössbauer spectral study of ferruginous one-layer trioctahedral micas. American Mineralogist, 71, 951–961.

Dyar, M.D., Colucci, M.T., and Guidotti, C.V. (1991) Forgotten major elements: Hydrogen and oxygen variation in biotite from metapelites. Geology, 19, 1029–1032.

Evans, B.W., Johannes, W., Otterdoom, H., and Trommsdorff, V. (1976) Stability of chrysotile and antigorite in the serpentine multisystem. Schweizerische mineralogische und petrographische Mitteilungen, 56, 79–93.

Frost, B.R. (1985) On the stability of sulfides, oxides and native metals in serpentinite. Journal of Petrology, 26, 31–63.

——— (1991) Magnetic petrology and factors that control the occurrence of magnetite in crustal rocks. In Mineralogical Society of America Reviews in Mineralogy, 25, 489–509.

Glen, R.A., and Butt, B.C. (1981) Chrysotile asbestos at Woodsreef, New South Wales. Economic Geology, 76, 1153–1169.

Guggenheim, S., and Eggleton, R.A. (1985) Modulated 2:1 layer silicates: Review, systematics and predictions. American Mineralogist, 72, 724–738.

Jensen, S.D., and Shive, P.N. (1973) Cation distribution in sintered titanomagnetites. Journal of Geophysical Research, 75, 8474–8480.

Lamarche, R.Y. (1973) Geology of the asbestos ophiolite complex, southern Québec. G.M. 28558, Québec Department of Natural Resources, Québec City.

Malysheva, T.V., Grachev, V.I., and Chashchukhin, I.S. (1976) Study of Ural serpentines by Mössbauer spectroscopy. Geokhimiya, 4, 612–625.

Mellini, M. (1982) The crystal structure of lizardite *1T*: Hydrogen bonds and polytypism. American Mineralogist, 67, 587–598.

Mellini, M., and Zanazzi, P.F. (1987) Crystal structures of lizardite *1T* and lizardite *2H*$_1$ from Coli, Italy. American Mineralogist, 72, 943–948.

Nagy-Czabo, I., Vertes, A., Music, S., Hadzija, O., Dracevic, Z., and Lahhodny-Sarc, O. (1981) ^{57}Fe Mössbauer analysis of chrysotile asbestos from various mining regions. Acta Geologica Academiae Scientiarum Hungaricae, 24, 149–155.

O'Hanley, D.S. (1988) A reconnaissance study of the United asbestos deposit, Midlothian township, district of Timiskaming. Ontario Geological Survey, Miscellaneous Paper, 141, 219–221.

——— (1991) Fault-controlled phenomena associated with hydration and serpentine recrystallization during serpentinization. Canadian Mineralogist, 29, 21–35.

O'Hanley, D.S., and Offler, R. (1992) Characterization of multiple serpentinization, Woodsreef, New South Wales. Canadian Mineralogist, 30, in press.

O'Hanley, D.S., and Wicks, F.J. (1987) Structural control of sepentine textures in the Cassiar Mining Corporation's open-pit mine at Cassiar, British Columbia. Geological Association of Canada/Mineralogical Association of Canada Program with Abstracts, 12, 77.

Rozenson, I., Bauminger, E.R., and Heller-Kallai, L. (1979) Mössbauer spectra of 1:1 phyllosilicates. American Mineralogist, 64, 893–901.

Ruby, S.L. (1973) Why MISFIT when you have $\chi 2$? In I.J. Gruverman and C.W. Seidel, Eds., Mössbauer effect methodology, 8, p. 263–276. Plenum, New York.

Stone, A.J., Parkin, K.M., and Dyar, M.D. (1984) STONE: A program for resolving Mössbauer spectra. DEC User's Society Program Library, no. 11-720, Marlboro, Massachusetts.

Toft, P.B., Arkani-Hamed, J., and Haggerty, S.E. (1990) Petrophysics of retrograde serpentinization. Physics of the Earth and Planetary Sciences, 65, 137–157.

Whittaker, E.J.W., and Wicks, F.J. (1970) Chemical differences among the serpentine "polymorphs"—A discussion. American Mineralogist, 55, 1025–1047.

Wicks, F.J., and O'Hanley, D.S. (1988) Serpentines: Structures and petrology. In Mineralogical Society of America Reviews in Mineralogy, 19, 91–168.

Wicks, F.J., and Plant, G. (1979) Electron microprobe and X-ray microbeam studies of serpentine textures. Canadian Mineralogist, 17, 785–830.

Wicks, F.J., and Whittaker, E.J.W. (1975) A reappraisal of the structures of the serpentine minerals. Canadian Mineralogist, 13, 227–243.

Wicks, F.J., and Zussman, J. (1975) Microbeam X-ray diffraction patterns of the serpentine minerals. Canadian Mineralogist, 13, 244–258.

Manuscript received March 13, 1991
Manuscript accepted November 15, 1992